

Marinarium: a New Arena to Bring Maritime Robotics Closer to Shore

Ignacio Torroba¹, David Dörner¹, Victor Nan Fernandez-Ayala², Mart Kartasev³, Joris Verhagen³, Elias Krantz¹, Gregorio Marchesini², Carl Ljung¹, Pedro Roque⁴, Chelsea Sidrane³, Linda Van der Spaa², Nicola De Carli², Petter Ögren³, Christer Fuglesang¹, Jana Tumova³, Dimos V. Dimarogonas² and Ivan Stenius¹

¹Division of Aerospace, Moveability and Naval Architecture, Royal Institute of Technology, 10044 Stockholm, Sweden

²Division of Decision And Control Systems, Royal Institute of Technology, 10044 Stockholm, Sweden

³Division of Robotics, Perception and Learning, Royal Institute of Technology, 10044 Stockholm, Sweden

⁴Division of Engineering and Applied Science, California Institute of Technology, Pasadena, CA 91125, USA

Corresponding author: Ignacio Torroba (email: torroba@kth.se).

This work was partially supported by Digital Futures, Vinnova and FMV through the SHARCEX grant and by the Wallenberg AI, Autonomous Systems and Software Program (WASP) funded by the Knut and Alice Wallenberg Foundation.

ABSTRACT This paper presents the Marinarium, a modular and stand-alone underwater research facility designed to provide a realistic testbed for maritime and space-analog robotic experimentation in a resource-efficient manner. The Marinarium combines a fully instrumented underwater and aerial operational volume, extendable via a retractable roof for real-weather conditions, a digital twin in the SMaRCSim simulator and tight integration with a space robotics laboratory. All of these result from design choices aimed at bridging simulation, laboratory validation, and field conditions. We compare the Marinarium to similar existing infrastructures and illustrate how its design enables a set of experiments in four open research areas within field robotics. First, we exploit high-fidelity dynamics data from the tank to demonstrate the potential of learning-based system identification approaches applied to underwater vehicles. We further highlight the versatility of the multi-domain operating volume via a rendezvous mission with a heterogeneous fleet of robots across underwater, surface, and air. We then illustrate how the presented digital twin can be utilized to reduce the reality gap in underwater simulation. Finally, we demonstrate the potential of underwater surrogates for spacecraft navigation validation by executing spatiotemporally identical inspection tasks on a planar space-robot emulator and a neutrally buoyant Remotely Operated Vehicle (ROV). In this work, by sharing the insights obtained and rationale behind the design and construction of the Marinarium, we hope to provide the field robotics research community with a blueprint for bridging the gap between controlled and real offshore and space robotics experimentation.

INDEX TERMS Autonomous Underwater Vehicles (AUVs), field robotics infrastructure, space robotics.

I. INTRODUCTION

RESearch and development of maritime robotics has traditionally lagged behind its ground and aerial counterparts [1]. The reasons for this gap are manifold: i) the complexity and risks associated with deploying and recovering robots offshore, which makes testing maritime technology intrinsically more costly and inaccessible, ii) the limited observability and weather-dependent repeatability of experiments carried out in open water, which hinders a rigorous evaluation and benchmarking of results, and iii) the reduced ability to compile large-scale datasets underwater

(UW) with accurate ground truth, a foundational block of machine learning [2].

To bypass these limitations, researchers in marine robotics often resort to simulators as widely accessible surrogates of the marine domain. The recent boom in open-source UW simulators is an eloquent sign of this trend [4, 5, 6]. However, the complexity of accurately modeling hydrodynamic interactions, acoustic and electromagnetic propagation, and open water conditions results in large differences remaining between the simulation and the real open water domain. These differences, known as the simulation to real (Sim2Real) gap

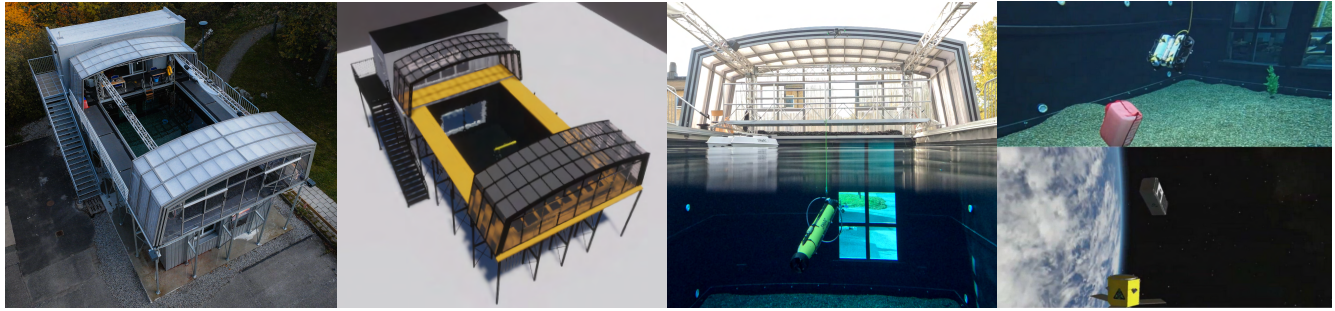


FIGURE 1. From left to right: i) aerial view of the Marinarium facility, ii) the facility digital twin in the SMarCSim, iii) multi-domain operational volume inside and iv) equivalent inspection tasks executed by a BlueROV2 in the tank and a simulated CubeSat in Basilisk [3].

[7], severely limit the fidelity of this type of simulators and thus hinder the deployment of systems developed in simulation into the real world, resulting in underwater robotics research often remaining in the simulation realm [8, 9]. Water tank facilities are often used as an intermediate development step between simulation and deployment in the real maritime environment [10, 11]. They can serve as a proxy of the offshore domain with controllable and observable conditions, reducing testing risks and enabling repeatability of the experiments. There is a large body of work containing instances of water tank facilities used as testbeds for experimentation in guidance, navigation and control of underwater vehicles [12, 13, 14], multi-domain collaboration with heterogeneous fleets [10] or deployment of control policies trained in simulation [15, 16, 17]. Analogously, water tank facilities can also serve as accessible test environments for space robotics [18, 19]. Neutral buoyancy conditions underwater provide a useful approximation of microgravity, allowing experimentation and testing under reduced weight effects and continuous, low-damping motion [20, 21]. However, despite the above advantages, water tank research facilities continue to be scarce due to their elevated installation and operational costs and thus their accessibility to the scientific community remains insufficient.

To ameliorate this, we present the Marinarium, a newly designed underwater robotics research facility at KTH Royal Institute of Technology (KTH). The Marinarium, in Figure 1, is a low-cost, self-contained and modular infrastructure consisting of a $9 \times 5 \times 3$ m water basin above the ground with a $9 \times 5 \times 2$ m drone space above the surface and a control room directly connected. The resulting operational volume is housed by a fully retractable ceiling to provide real weather conditions during surface and air operations, and it is fully monitored both above and underwater via two Motion-Capture Systems (MoCaps).

We argue that the following four design aspects are key to the novelty and utility of the Marinarium to the research community:

- A novel modular design for a cost-effective, standalone underwater research facility, enabling affordable, long-term experimentation and data collection.

- A combined air and underwater operating volume, monitored with two MoCap systems and with access to the open air through a retractable dome, creating the ideal arena for inter-domain experimentation in air, surface and underwater robotics.
- A digital twin of the facility in the SMarCSim UW simulator [5], providing a perfect framework for Sim2Real research on underwater perception and actuation.
- A tight integration with the KTH space robotics laboratory [22], resulting in a well-suited testbed to study and exploit the commonalities between robotic platforms in space and underwater conditions.

In this work, we present the Marinarium and compare it to existing state-of-the-art facilities. We then showcase its potential to help bring realistic maritime robotics closer to the research and academic community by presenting novel results in four open-research areas from experiments enabled by the facility: data-driven System Identification (SYSID) for underwater vehicles, heterogeneous, multi-domain maritime robotics, underwater Sim2Real bridging, and space robotics validation via underwater surrogates.

II. RELATED WORK

In this section, we present an overview of research facilities similar to the Marinarium around the globe. Subsequently, we introduced related work in the four different research areas in which tank-based experiments have been executed.

A. EXISTING MARINE ROBOTICS RESEARCH FACILITIES

Based on their environmental scope, existing maritime robotics research facilities range from large natural outdoor areas for field testing to small indoor, fully-monitored basins with controlled conditions. On the one side of this range, facilities such as the MBARI MARS system [40], the Fraunhofer Digital Ocean Lab (DOL) in the Baltic Sea [41], and the NTNU and SINTEF Fjordlab [42] provide sensors for environmental monitoring and robotics development. The DOL and Fjordlab complement stationary platforms with instrumented surface and underwater vehicles.

TABLE 1. Similar underwater robotics research facilities worldwide and their main characteristics regarding location, volume, control of water conditions, motion tracking capabilities underwater (UW), additional connected above-water (AW) capabilities, suitability for divers –where ‘-’ indicates a potential but not-known experiments involving divers–, and research focus. The following additional abbreviations are employed: RGB cameras (RGB), Ultra-Wideband localization (UWB), Unmanned Surface Vehicle (USV), Unmanned Aerial Vehicle (UAV).

Institution	Location	L×W×D or ∅×D (m)	Control	UW	AW	Divers	Type of Research
SINTEF [23]	Norway	80 × 50 × 10	Wave, Wind, Current	MoCap, RGB	MoCap, RGB	-	UW/Surface Structures, AUVs
TCOMS [24]	Singapore	60 × 48 × 12	Wave, Current	-	MoCap	no	UW Structures, Robotics
deep pit		∅10 × 50		-	-	no	
Ifremer [25]	France	50 × 12.5 × 20	Wave, Wind	MoCap, RGB	MoCap, RGB	yes	Hydrodynamics, UW Structures, Robotics incl. Diver Collab.
Aquatron, Pool Tank [26]	Canada	∅15.24 × 3.91	Temperature, Current	-	Drone space	-	Marine Life, Multi-Domain, Robotics, Sensors [10]
Tower Tank		∅3.66 × 10.46	Current	-	-	-	Pressure Activated Instruments
Pools 1,2,3		9.1 × 7.3 × 4	Current	-	-	-	AUVs, USVs
CalTech [27]	USA	4.8 × 1.8 × 1.5	Current	-	-	no	UW Robotics
UMich [28]	USA	5.18 × 3.05 × 1.98		MoCap	MoCap		AUVs, USVs, UW Robotics
FRoSt [29]	USA	9.14 × 6.10 × 1.83		-	-	-	AUVs
JHU [12]	USA	∅7.49 × 3.96		-	-	-	AUVs, Robotics
NBRF [30, 31]	USA	∅15.24 × 7.62		MoCap, RGB	-	yes	Space/UW Robotics
NBL [32]	USA	61.5 × 31.1 × 12.2	Temperature, Wind, Wave	MoCap	MoCap	yes	Astronaut Training/Medical Research
EAC [20]	Germany	22 × 17 × 10		-	-	yes	Astronaut Training
DFKI [33]	Germany	23 × 19 × 8		MoCap	RGB	yes	Space/UW Robotics
glass tank		5 × 4 × 2.2		-	-	no	UW Robotics
black tank		3.4 × 2.6 × 2.2	Turbidity	-	-	no	UW Robotics
AST [34]	Germany	12 × 8 × 3		-	-	-	UW Robotics
CIRS [35]	Spain	16.5 × 9.5 × 5		RGB	-	-	UW Robotics, UW Vision
CIRTESU [36]	Spain	12 × 8 × 5	Current, Wave	-	-	-	UW Robotics, Vision, Wireless Comm., Teleop., Fluids
ISEP [37]	Portugal	10 × 6 × 5		RGB	-	-	USVs, UW Robotics
LABUST [11]	Croatia	7.8 × 4.1 × 3		RGB	RGB, UWB, space for micro-UAV	-	UW Robotics
AAU [38]	Denmark	7.5 × 3.6 × 1.5		MoCap	-	-	USVs, UW Robotics
black tank		1.2 × 1.2 × 2.3	Acoustic damping	-	-	no	Perception
ASTA [39]	Denmark	6.5 × 3.5 × 3	Current	-	MoCap, 16×12×8 m Drone cage	no	Multi-Domain Collab. Robotics

However, while extremely valuable, such facilities are very scarce due to their large scale and operational complexity and therefore fail to directly contribute to the democratization of underwater robotics research. On the other side of the spectrum, smaller indoor water tanks such as the Marinarium are more widely used in academic research due to their simpler setup and affordability. In Table 1, we compiled a list of representative facilities and highlighted, for comparison, their main characteristics in terms of size and location, existing equipment and intended use.

Regarding the size of the facility, the water basins housed by SINTEF Ocean [23], TCOMS [24], Ifremer [25] and the Neutral Buoyancy Laboratory (NBL) [32] at NASA’s Johnson Space Center (JSC) are among the largest in the world. On the scale of the Marinarium, North American universities house UW tanks at Caltech [27], Dalhousie University [26], University of Michigan [28], Brigham Young University [29], and John Hopkins University [12]. In mainland Europe, similar infrastructures for UW robotics testing are found at the Fraunhofer Institute for Applied Systems

Engineering [34] in Germany; CIRS [35] at the University of Girona and CIRTESU [36] at the University Jaume I in Spain; at INESC TEC ISEP [37] in Portugal; LABUST [11] at the University of Zagreb, Croatia; and at Aalborg University [38] and the Autonomous Systems Test Arena (ASTA) at the Technical University of Denmark (DTU) [39].

MoCap systems are used for high-quality data collection and tracking both underwater [23, 25, 28, 31, 33] and on air [23, 24, 25, 28, 39]. However, of these facilities, only three include systems in both domains [23, 25, 28] as the Marinarium does, creating an ideal setup for multi-domain collaborative robotics development.

Concerning controllable water conditions, only the largest facilities among the above [23, 24, 25] can house wave and/or wind generators for realistic seafaring conditions. Current control, on the other hand, is easier to achieve and is therefore a more common feature in smaller ones [26, 27, 36, 39]. Water turbidity regulation is useful to mimic realistic visibility conditions for testing of vision-based navigation systems. However, the performance of underwater MoCap systems is highly dependent on the clarity of the water volume and therefore only a smaller dedicated tank [33] offers this feature.

Focusing on space robotics, the larger Neutral Buoyancy Research Facility (NBRF) at the University of Maryland [31] was originally built to study orbital operations to support NASA, but is now also equipped for UW robotics research. Its counterpart in Europe is the test facility at DFKI Bremen [33], intended for both UW and space robotics [19]. The neutral buoyancy labs at NASA [32] and the European Space Agency (ESA) [20] focus primarily on astronaut training. To the best of our knowledge, none of the small or medium-sized facilities incorporate infrastructure for combined underwater and space robotics research.

Regarding digital representations of the facilities, while several of them have accompanying simulation environments modeling some aspects of their water tanks [10, 11, 32, 33, 35], the only published literature found that demonstrates a digital twin of any of the indoor UW research facilities is CIRTESU [43].

In addition to the specialized facilities listed, examples of towing tanks [14, 17, 44], and swimming pools [13, 45, 46] employed ad-hoc for UW robotics testing are common in the literature, which is a sign of both the scarcity of these specialized facilities and their value to this research.

B. UNDERWATER VEHICLE DYNAMICS MODELING

Vehicle dynamics models are an essential building block for control design, state estimation or simulation techniques. The modeling of maritime vehicles has traditionally relied on Computational Fluid Dynamics (CFD) methods or data from resistance and self-propulsion tests from scaled-down models in a towing tank [47]. However, data-driven techniques are becoming increasingly popular as a lighter and more cost-effective alternative to these methods [48].

Regarding first-principle methods, the study in [49] estimated hydrodynamic coefficients from basic geometry and mass properties for a BlueROV2, whereas the work in [50] carried out an extensive system-identification campaign to obtain more reliable parameters. Both works highlight that accurate added-mass and damping estimation requires controlled experiments and is difficult to maintain across vehicle configurations, motivating data-driven alternatives.

The review in [51] surveys Artificial Intelligence (AI) methods for underwater navigation and control and under-line model learning as a key trend. Early applied work such as [52] used Support Vector Regression to capture coupled AUV dynamics from onboard logs. More recently, the approach in [48] proposed a Physics-informed Neural network with control (PINc) for BlueROV2 modeling and, in [53], a dynamic-forgetting Gaussian Process (GP) residual model embedded in Model Predictive Control (MPC), which augments, rather than replacing, a physics baseline. As an alternative, Koopman operator approaches, like Extended Dynamic Mode Decomposition with control (EDMDc), provide linear, control-coherent surrogates; e.g., [54] demonstrated accurate predictive control for a nonlinear robotic manipulator. The controlled instrumented environment provided by the Marinarium enables the collection of the dense, low-noise state-input datasets required for such data-driven operator-theoretic system identification. To our knowledge, this work is the first example of the Koopman operator being applied in underwater robotics.

C. MULTI-DOMAIN HETEROGENEOUS MARITIME ROBOTICS

Multi-domain robotic systems involve coordination between autonomous platforms in more than one of the following domains: underwater, water's surface, land, air, and space [55, 56]. This type of system is increasingly important offshore because seaborne transportation accounts for more than 80% of global trade volume [57], and the digitalization and automation of maritime activities, environmental monitoring, and search and rescue operations are relying more heavily on fleets of heterogeneous autonomous platforms [58, 59, 60]. Traditionally, given their operational complexity, these types of multi-robot systems have been developed and tested in simulation [61], directly offshore [55, 58], or via a combination of both [59, 60]. We argue that further testing in controlled facilities, as an intermediate step, can save costly field testing time and speed up development. However, there are not many examples of this type of indoor experimental setup [10]. We showcase how the Marinarium provides a unique multi-domain arena for this type of experimental development through the execution of a multi-domain mission with a heterogeneous fleet of robots.

D. UNDERWATER SIM2REAL GAP BRIDGING

Although state-of-the-art simulators still fail to fully capture real-world physics accurately (the so-called simulation-to-

real gap), the latest advances in sim2real bridging techniques [7] have demonstrated the feasibility of successfully deploying control policies developed entirely in simulation directly into real-world hardware [62]. However, the intrinsically higher complexity of modeling hydrodynamics accurately has hindered achieving a similar level of success in bridging the sim2real gap in the underwater domain. The performance deterioration caused by this gap can be seen in the fact that many underwater reinforcement learning works remain in the simulation realm [8, 9], or are tested in real hardware only under very limited conditions [15, 63]. A practical alternative to more accurate but computationally expensive hydrodynamic simulators is the use of residual dynamics models to complement the simulated robot dynamics, as demonstrated in [64, 65]. Residual models capture the discrepancy between simulated and real-world vehicle motion, and subsequently enhance the fidelity of the simulator. However, learning these residuals requires access to high-accuracy, real-world motion data paired with the simulated vehicle to be enhanced, which has prevented this technique from being applied to underwater simulators. To bridge this gap, in this work we combine the Marinarium with its digital twin in the SMARCSim and demonstrate how residual dynamics regression can be applied to improve underwater dynamics simulation.

E. SPACE VALIDATION UNDERWATER

Neutral buoyancy environments have long served as microgravity surrogates for space research, supporting both astronaut training and robotic testing in facilities such as NASA’s Neutral Buoyancy Laboratory [32] and the University of Maryland’s Neutral Buoyancy Research Facility [30]. Several underwater spacecraft analogs were developed in these settings, including SCAMP [66], Ranger [18], and EUCLID [67], demonstrating that underwater vehicles can emulate free-flying spacecraft behavior for inspection, servicing, and control studies. Despite their early success, this line of research has seen limited continuation. Simultaneously, planar air-bearing testbeds have become the standard for ground-based emulation of spacecraft dynamics. One such air-bearing testbed is the Autonomy Testbed for Multi-purpose Orbiting Systems (ATMOS) [22], located at KTH.

To the best of the authors’ knowledge, NASA JSC is the only other facility housing both an UW lab and a precision air bearing floor for space experiments [68]. The Marinarium is smaller in size, but comes with UW MoCap for ground truth positioning. Furthermore, the Marinarium and its robots have been designed to run the same software stack as ATMOS to facilitate parallel space-simulation experiments between the two facilities. Each emulation facility has different strengths for simulating space missions, such as the Marinarium’s ability to simulate 3D motions and ATMOS’s ability to simulate drag-free planar motion. Together, these facilities provide a unique testing environment.

In the remainder of this work, we introduce the Marinarium capabilities in Section III, and then showcase, through a set of experiments, four key open-research areas within field robotics that it facilitates, namely: i) data-driven system identification of underwater vehicles in Section IV, ii) sim2real gap bridging for underwater simulation in Section VI, iii) multi-domain maritime robotics testing under controlled conditions in Section V and iv) validation of space robotics using underwater surrogates in Section VII.

III. THE MARINARIUM FACILITY

The Marinarium has been designed with modularity and resource-efficiency at its core. To this end, it is comprised of pre-built sections that can be assembled, disassembled, and modified as needed. It consists of three main modules: i) an overground 3 m deep water basin of 9×5 m, ii) two stacked office modules with direct access to the surface of the pool from the top module and large underwater windows into the water volume in the bottom module, and iii) a freestanding terrace at water surface level with a retractable roof. These three components have been combined to create a standalone facility that can house equipment and carry out long-term experiments under repeatable and stable conditions. The CAD model and main plans can be seen in Figure 2. Owing to these design choices, the overall construction costs of the facility (not including the MoCap systems) is estimated to be under 4M Swedish krona.

A. MULTI-DOMAIN OPERATING WORKSPACE

The Marinarium water basin has a total volume of 135 m^3 . A Qualisys underwater MoCap system with 8 Arqus cameras and 1 Miquis video camera has been installed just below the surface to provide full coverage of the basin. The camera setup can be seen in Figure 5. A truss system has been set up along the perimeter of the basin to enclose a $9 \times 5 \times 2$ m area over the water that can be fully confined and monitored. Alternatively, this volume can be expanded into the open air through the retractable roof, allowing experiments to be carried out under real meteorological conditions closer to the real world. For tracking in the volume over the water surface, an Optitrack MoCap system with up to 16 Flex 13 cameras can be set up and reconfigured on the truss system. The Qualisys and Optitrack MoCap systems are integrated through Robot Operating System (ROS) 2.

B. UNDERWATER ACOUSTIC PERFORMANCE

The water basin consists of a steel skeleton supporting a 20 mm PE100 RC liner that houses 135 t of water. To improve the acoustic properties of the water volume, the bottom is covered with 3 t of yellow-mottled sea gravel of 8-16 mm radius (Figure 3). The stones scatter acoustic reflections from sonar instruments and reduce multipathing in low-frequency instruments in a tank of these dimensions. As an example, the use of these stones has enabled a

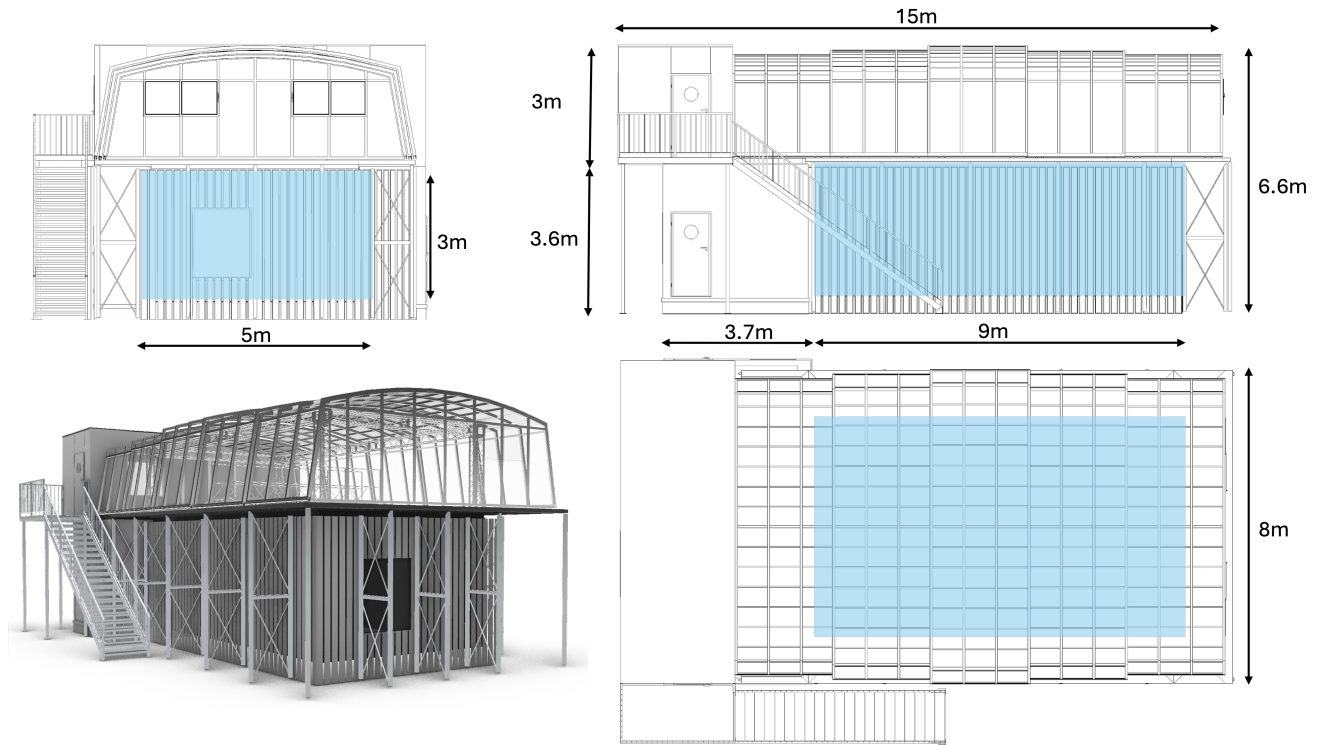


FIGURE 2. Plans and CAD model of the Marinarium with the dome closed. The structure is built combining pre-fabricated modules, a floating terrace at water surface level and a retractable roof, to form a stand-alone facility. The $9 \times 5 \times 3$ m water basin volume has been depicted in blue for visualization purposes.

transmission rate of 70% with Delphis Succorfish modems (24-32 kHz acoustic frequency), from a 0% without stones.

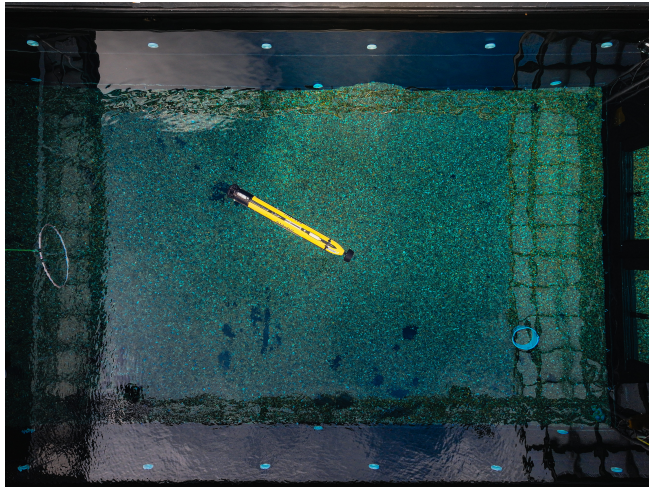


FIGURE 3. Partial aerial view of the Marinarium water basin. 3 tones of sea gravel of 8-16 mm radius have been laid on the floor to reduce acoustic multipath and enable the operation of low-frequency acoustic equipment.

C. WATER TREATMENT SYSTEMS

The tank has been instrumented to preserve water conditions within operating ranges in terms of clarity for the Qual-

isys MoCap, sanitation for diving work, and temperature control for infrastructure maintenance. The equipment consists of two equivalent and independent piping subsystems for robustness. Each of them encompasses a chlorination dispenser, an Ultraviolet (UV) disinfection unit, a sand-based filter, and a heating system. Two heat pumps provide an actionable water temperature range of 6-40 °C. Their purpose is two-fold: i) to keep the water within the operating temperature of the Qualisys cameras, 0-35 °C, and ii) to prevent pipes from freezing during winter. Regarding sanitation, the automatic chlorination dispenser maintains the water quality within the working standards for human use, while the water clarity is maintained to optimize the MoCap measurement distances via two 800 kg sand filters. Finally, two UV-C cleaners are used to both disinfect the water and photodegrade the chlorine byproducts, which are known to increase water turbidity.

D. DIGITAL TWIN

The digital twin of the Marinarium facility has been implemented in the SMARCSim simulator [5], and can be seen in Figure 1. This replica of the facility is integrated with the real infrastructure via a ROS 2-Unity bridge. Through this bridge, the real-time state of the vehicles in the environment, both from the MoCaps and their internal estimators, can be directly forwarded into the simulator. These digital representations of the real vehicles in the simulation can

then be directly compared to their simulated counterparts. Equivalently, this setup enables seamless Software-in-the-loop (SIL) testing from the simulator into the real vehicle prior integration into the real hardware.

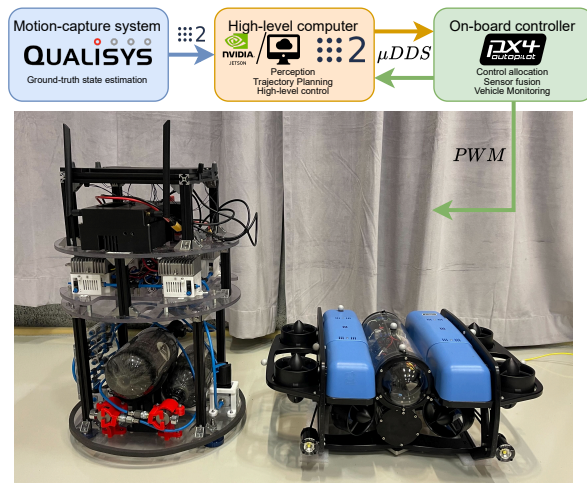


FIGURE 4. The ATMOS free-flyer [22], the BlueRobotics BlueROV2 Heavy, and their identical autonomy stack. Ground truth state estimation is obtained from a Qualisys MoCap system and transferred to either an on-board Nvidia Jetson or an off-board PC via ROS 2. High-level computing and decision-making is performed in ROS 2 after which high-level control signals are sent to an onboard PixHawk microcontroller which allocates the control to the individual actuators.

E. INTEGRATION WITH THE KTH SPACE ROBOTICS LAB

The Marinarium is located adjacent to the KTH space robotics laboratory [22], within the campus of KTH. The geographic proximity allows the facilities to both share resources and be connected through an optical fiber network, enabling them to operate in the same ROS 2 domain and carry out combined experiments. Furthermore, in order to build an underwater surrogate platform of the ATMOS free-flyer [22] vehicles in the space robotics laboratory, a set of BlueRobotics BlueROV2 Heavy have been equipped with an identical software and control stack. Each robot is equipped with a Pixhawk 6X–Mini microcontroller running PX4 [69], which performs onboard sensor fusion of inertial and external motion-capture data and computes low-level control by allocating commanded forces and torques to the actuators. PX4 provides modular configuration, robust control features, and native integration with ROS 2, ensuring consistent control logic and data handling across both platforms. All communication, supervision, and data logging are handled through ROS 2.

IV. DATA-DRIVEN SYSID FOR UW VEHICLES

Accurate dynamics models are central to navigation, control, and simulation of underwater vehicles. They provide the predictive baseline for controller design, state estimation, and pre-deployment testing and validation. We begin by recalling the physics-based formulation commonly used in underwater robotics.

A. UNDERWATER VEHICLE DYNAMICS

The dynamics of underwater vehicles are typically described via the standard Fossen model [70] as:

$$M\dot{\boldsymbol{\nu}} + C(\boldsymbol{\nu})\boldsymbol{\nu} + D(\boldsymbol{\nu})\boldsymbol{\nu} + g(\boldsymbol{\eta}) = \mathbf{w}(\mathbf{u}), \quad (1)$$

where $\boldsymbol{\eta} = [x, y, z, \phi, \theta, \psi]$ is the AUV pose in the inertial frame and $\boldsymbol{\nu} = [u, v, w, p, q, r]$ is the body-frame velocity twist. The inertia matrix is given by $M = M_{RB} + M_A$, which combines the rigid-body and added-mass contributions. Similarly, the Coriolis and centripetal terms are grouped in $C(\boldsymbol{\nu}) = C_{RB}(\boldsymbol{\nu}) + C_A(\boldsymbol{\nu})$, whereas $D(\boldsymbol{\nu})$ denotes the hydrodynamic damping forces. The term $g(\boldsymbol{\eta})$ captures the gravitational and buoyancy restoring forces, and $\mathbf{w}(\mathbf{u})$ is the actuated wrench. In practice, this wrench is not directly actuated; instead, it is obtained from the individual thruster and actuator inputs, denoted as \mathbf{u} .

Despite the widespread use of the Fossen model in Equation (1), obtaining an accurate and reliable parameterization of the model remains difficult in practice. In particular, the hydrodynamic damping coefficients in $D(\cdot)$ and the added-mass terms in M_A are challenging to identify due to strong coupling effects, nonlinear velocity dependence, and sensitivity to operating conditions [70]. Furthermore, the resulting models are sensitive to weight and buoyancy trimming, fairing, payload reconfiguration, and seemingly minor configuration choices. Such factors are unavoidable during real deployments, making models based on a static parameter set, e.g., [50], unreliable and difficult to validate across slightly different vehicles and domains. This motivates a data-driven surrogate of Equation (1) that (i) identifies the effective closed-loop dynamics under the as-sailed configuration, and (ii) can be rapidly re-fit after hardware changes.

B. DATA-DRIVEN DYNAMICS MODELING

In this work, we propose to identify a discrete-time dynamics model of the underwater robot directly from data. The Marinarium provides a controlled and repeatable testing environment, allowing the collection of high-fidelity datasets from an instrumented BlueROV2 (Figure 5). For this study, we recorded three datasets of more than 15 min each, containing synchronized measurements of the full 12-dimensional vehicle state and the 8 thruster command channels. Some datasets contain limitations on the pitch and roll movements to ensure a fair comparison with the 4-DoF-based models, e.g., [48], while others contain full 6-DoF motion.

The state vector, comprising position, orientation, and linear and angular body-frame velocities, is defined as

$$\mathbf{x} \doteq [\boldsymbol{\eta}^T, \boldsymbol{\nu}^T]^T \in \mathbb{R}^{12},$$

and the input $\mathbf{u} \in [-1, 1]^8$ are the individual BlueROV2 motor commands. The data for states and inputs is obtained from the underwater MoCap (pose and odometry), onboard Inertia Measurement Unit (IMU) (angular rates/linear acceleration), and controller logs (thrusters). After data collection, we sort measurements by timestamp, remove duplicates and NaNs, and resample to 50 Hz (median sample time $\Delta_t \approx$

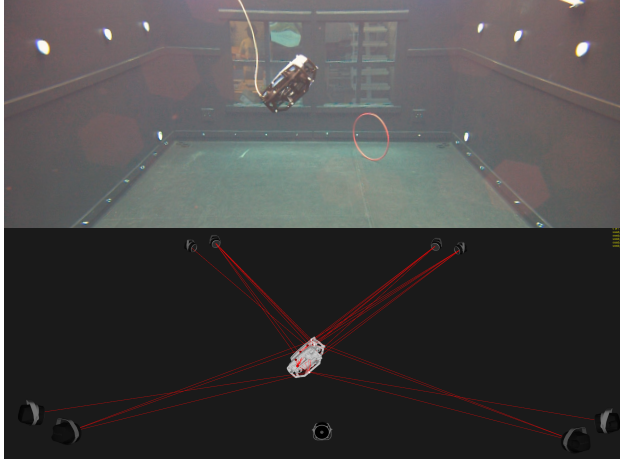


FIGURE 5. The BlueROV2 Heavy in the Marinarium during the data collection for sysID (top). The vehicle state x_k is provided by the Qualisys motion capture system (bottom).

0.02 s), yielding more than 45823 time-aligned samples per dataset. Unless otherwise stated, splits are chronological (first 80% train, last 20% test) to avoid leakage.

C. BASELINES AND MODELS

In the following, we compare four models trained on the same dataset. Let $R(\phi, \theta, \psi) \in \mathbb{R}^{3 \times 3}$ denote the rotation matrix from the body frame (b) to the inertial/navigation frame n , constructed from ZYX Euler angles $\boldsymbol{\mu} = [\phi, \theta, \psi]^\top$. We partition the state in position $\mathbf{p} = [x, y, z]^\top$, euler angles $\boldsymbol{\mu}$, linear velocity $\mathbf{v} = [u, v, w]^\top$, and angular velocity $\boldsymbol{\omega} = [p, q, r]^\top$.

Double Integrator-like (DI) in the body frame

Under a small-angle approximation for roll and pitch, the Euler-angle kinematics simplify to

$$\dot{\boldsymbol{\mu}} \approx \boldsymbol{\omega} \quad (2)$$

which yields a first-order attitude update and removes the trigonometric coupling between angular rates and Euler-angle derivatives. In this regime, the vehicle's translational and rotational dynamics can be approximated as body-frame double integrators driven by the thruster inputs. We model the input–acceleration relationship by estimating constant gain matrices

$$K_{\text{lin}}, K_{\text{ang}} \in \mathbb{R}^{3 \times 8}$$

using ridge-regularized least squares (Tikhonov regularization [71]). These matrices map the 8 thruster commands to linear and angular accelerations:

$$\dot{\mathbf{v}} \approx K_{\text{lin}} \mathbf{u}, \quad \dot{\boldsymbol{\omega}} \approx K_{\text{ang}} \mathbf{u},$$

where the Coriolis term is missing since only small angular velocities are considered. Using an explicit forward Euler integration step with sampling time Δ_t , the resulting discrete-

time dynamics become

$$\mathbf{p}_{k+1} = \mathbf{p}_k + \Delta_t R(\phi_k, \theta_k, \psi_k) \mathbf{v}_k, \quad (3)$$

$$\boldsymbol{\mu}_{k+1} = \boldsymbol{\mu}_k + \Delta_t \boldsymbol{\omega}_k. \quad (4)$$

$$\mathbf{v}_{k+1} = \mathbf{v}_k + \Delta_t (K_{\text{lin}} \mathbf{u}_k), \quad (5)$$

$$\boldsymbol{\omega}_{k+1} = \boldsymbol{\omega}_k + \Delta_t (K_{\text{ang}} \mathbf{u}_k), \quad (6)$$

Fossen (BlueROV2)

We adopt the BlueROV2 dynamics model from [50], using the nominal parameters reported therein. The continuous-time equations are integrated using a single explicit Euler step with sampling time Δ_t . No additional tuning or parameter adaptation is performed

Physics-informed Neural network with control (PINc)

Using the approach described in [48], we trained a network with our dataset using 1000 epochs and a loss of 1.9208. Notably, the loss did not seem to reduce significantly during the training, even though we used the same hyperparameters described in [48].

Koopman EDMDc with Radial Basis Function (RBF) dictionary (ours)

Following [72], we lift the state to a higher-dimensional *observable space* via a dictionary of functions $\theta(\cdot)$:

$$\mathbf{z} \doteq \theta(\mathbf{x}) = \begin{bmatrix} \mathbf{x} \\ \varphi_1(\mathbf{x}) \\ \vdots \\ \varphi_K(\mathbf{x}) \end{bmatrix} \in \mathbb{R}^{n+K}, \quad (7)$$

Here, the *observable space* refers to the space of functions of the state that we choose as basis. By lifting the state into this space, nonlinear dynamics in the original state can be approximated as linear dynamics in \mathbf{z} .

The additional coordinates $\varphi_i(\mathbf{x})$ are Gaussian RBFs:

$$\varphi_i(\mathbf{x}) = \exp(-\gamma \|\mathbf{x} - \mathbf{c}_i\|_2^2), \quad (8)$$

where K is the dictionary size, $\gamma > 0$ is a width parameter, and the centers $\{\mathbf{c}_i\}_{i=1}^K$ are selected from the training data using k -means clustering (details later). The dynamics in the lifted space are modeled as a linear, control-affine system

$$\mathbf{z}_{k+1} = A \mathbf{z}_k + B \mathbf{u}_k, \quad \mathbf{x}_k = C \mathbf{z}_k, \quad (9)$$

with C typically chosen to extract the original state coordinates from the lifted vector, and is typically referred to as *decoder* matrix. The matrices A and B are estimated via ridge-regularized least squares:

$$\min_{A, B} \|\Theta(Y) - [A \ B] [\Theta(X)^\top \ U^\top]^\top\|_F^2, \quad (10)$$

where $\|\cdot\|_F$ denotes the Frobenius norm, matrices $\Theta(X) = [\theta(x_0), \theta(x_1), \dots, \theta(x_{T-1})]$, $U = [u_0, u_1, \dots, u_{T-1}]$ and $\Theta(Y) = [\theta(x_1), \theta(x_2), \dots, \theta(x_T)]$. Equation (10) also admits the closed-form solution

$$[A \ B] = \Theta(Y) G^\top (G G^\top + \lambda I)^{-1}, \quad (11)$$

Algorithm 1 EDMDc-RBF identification for BlueROV2

- 1: **Input:** Snapshot tuples $\{(\mathbf{x}_k, \mathbf{u}_k, \mathbf{x}_{k+1})\}_{k=0}^{T-1}$, dictionary size K , RBF width γ , ridge λ .
- 2: **Centers (k-means):** Run k -means Equation (12) with K clusters on $\{\mathbf{x}_k\}$ to obtain centers $C = \{c_i\}_{i=1}^K$.
- 3: **Lift:** Define $\theta(\mathbf{x}) = [\mathbf{x}^\top, \varphi_1(\mathbf{x}), \dots, \varphi_K(\mathbf{x})]^\top$ using $\varphi_i(\mathbf{x})$ from Equation (8).
- 4: **Assemble:** $\Theta(X) = [\theta(\mathbf{x}_0), \dots, \theta(\mathbf{x}_{T-1})]$, $\Theta(Y) = [\theta(\mathbf{x}_1), \dots, \theta(\mathbf{x}_T)]$, and $U = [\mathbf{u}_0, \dots, \mathbf{u}_{T-1}]$.
- 5: **Ridge solve:** Form G and compute A, B with Equation (11).
- 6: **Decoder:** Set $C = [I_{12} \ 0]$ (or fit a linear decoder).
- 7: **Return:** (A, B, C) from Equation (9), centers C .

with $G = [\Theta(X)^\top U^\top]^\top$ and ridge parameter $\lambda > 0$. A simple decoder matrix $C = [I_{12} \ 0]$ is used, i.e., the first 12 lifted coordinates reconstruct \mathbf{x} , since using a learned decoder produced similar results in our tests. The full pipeline is shown in Algorithm 1.

The advantages of RBFs

Gaussian RBFs yield a universal and smooth basis on compact sets since linear combinations of RBFs are dense in the space of continuous functions defined on \mathcal{X} , denoted by $\mathcal{C}(\mathcal{X}) \doteq \{f : \mathcal{X} \rightarrow \mathbb{R} \mid f \text{ is continuous}\}$, and can therefore approximate polynomials and other smooth nonlinearities to arbitrary accuracy [73]. Practically, they provide locality, i.e., each φ_i characterizes a nonlinearity in the state dynamics in a local neighborhood of the corresponding center c_i . Such a feature helps to closely capture configuration-dependent effects like tether drag without hand-crafting cross terms. RBFs features are also linear in parameters, enabling the closed-form ridge solve in Equation (11).

k-means for RBF centers

Given training states $\{\mathbf{x}^{(j)}\}_{j=1}^N$, the k -means centers $\{c_i\}_{i=1}^K$ minimize within-cluster squared error:

$$\min_{\{c_i\}, \{\mathcal{C}_i\}} \sum_{i=1}^K \sum_{\mathbf{x}^{(j)} \in \mathcal{C}_i} \|\mathbf{x}^{(j)} - c_i\|_2^2, \quad c_i = \frac{1}{|\mathcal{C}_i|} \sum_{\mathbf{x}^{(j)} \in \mathcal{C}_i} \mathbf{x}^{(j)}, \tag{12}$$

where \mathcal{C}_i is the set of points assigned to center c_i and the random seed is fixed for reproducibility.

D. EVALUATION PROTOCOL

We report endpoint H -step Root Mean Square Error (RMSE) computed by rolling each model open loop (i.e., without re-initialization) under the recorded inputs:

$$\text{RMSE}_H \doteq \sqrt{\frac{1}{(N-H)n} \sum_{k=0}^{N-H-1} \|\mathbf{x}_{k+H} - \hat{\mathbf{x}}_{k+H|k}\|_2^2}, \tag{13}$$

for $H \in \{1, 10, 100\}$, state dimension $n=12$, $N = 9165$ being the total number of data points, and Euclidean norm

TABLE 2. Endpoint RMSE Equation (13) on recorded tank data for the full test data size of more than 9000 trajectories (lower is better).

Model	1-step	10-step	100-step
Koopman (EDMDc-RBF)	0.0629	0.0831	0.1859
Double Integrator-like (DI)	0.0784	0.1088	0.4683
Fossen (BlueROV2)	0.0765	0.2122	0.5788
PINc (ResDNN)	8.7886	9.1550	9.1639

$\|\cdot\|_2$. Note that Equation (13) calculates the average square error for all possible forward trajectories of size H started at the beginning of the test set until its near end, $N - H - 1$. For our test size of more than 3 min at 50Hz, this means we are averaging over more than 9000 diverse trajectories incorporating the widest possible variety of movements and starting conditions to reduce the model bias.

To ensure a fair comparison, all open-loop rollouts are performed with one-step Euler integration. An RK4-version was also analyzed with no noticeable differences. Hyperparameters for the Koopman model, (K, γ, λ) , were tuned via a small grid search on a subset of the training data and then fixed for the test set. The final selected values are $K = 500$, $\gamma = 3.0$, and $\lambda = 0.1$.

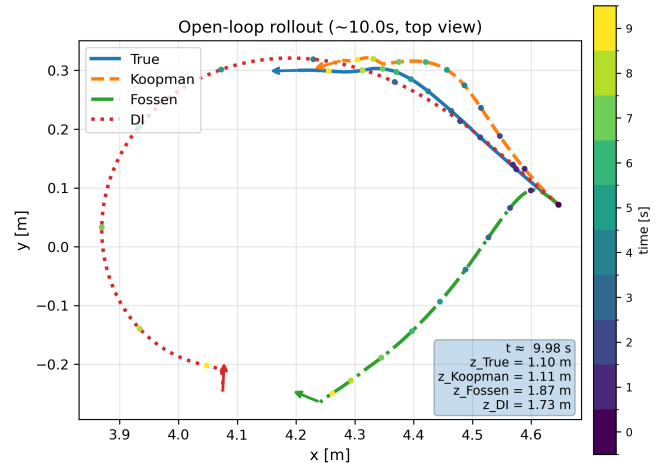


FIGURE 6. Recorded open-loop tank run (top view & depth) for 10s: ground truth vs. Koopman, physics and DI rollouts under identical inputs.

E. RESULTS AND DISCUSSION

Table 2 summarizes test-set performance. The Koopman model achieves the best accuracy at all horizons. The DI baseline is competitive at $H=1$ and $H=10$, but drifts more at $H=100$. The physics Fossen model from [50] starts in a similar range, but degrades quickly, consistent with small parameter mismatch under our tank configuration. Lastly, with the current hyperparameters, PINc does not seem to be able to learn a usable model for the underwater vehicle.

Figure 6 shows a top-view & depth (z) comparison for 10s of open-loop rollout. Note that we are neither showing the other six linear and angular velocity dimensions, nor

TABLE 3. Average training and rollout time for one step prediction.

Model	Rollout time [s]	Training time [s]
Koopman (EDMDc-RBF)	0.0800	4.617
Fossen (BlueROV2)	0.1535	-
Double Integrator-like (DI)	0.0105	0.004
PINc (ResDNN)	0.3265	482.269

the pitch and roll, but they have been taken into account for the RMSE computed in Table 2. Also note the enhanced difficulty in tracking since we are showing significantly more steps of open-loop evolution compared to previous works, which only considered less than 2 s of Interval of Valid Prediction (IVP) [48], i.e., when the real and replicated trajectory start diverging considerably (≥ 0.1 m). Qualitatively, the Koopman trajectory remains closest to ground truth while preserving heading evolution; DI follows closely, but overestimates forward speed and curvature during long yaw transients and misses on depth estimation; the physics rollout starts correctly, but diverges under the same inputs; while the PINc has been left out due to poor performance.

Runtime considerations

Although the lifted Koopman state has dimension $d = n + K > 500$, both training and rollout are computationally light: training is a single ridge solve Equation (11), and rollout is one matrix–vector multiply and an addition per step ($z_{k+1} = Az_k + Bu_k$) plus a cheap decode ($x_k = Cz_k$). In contrast, the physics baseline evaluates nonlinear hydrodynamic terms, thruster maps, and (when modeled) tether/delay dynamics, which increases per-step cost. The measured rollout and training times in Table 3, obtained on a desktop workstation (AMD Ryzen 7 5800 CPU, 32 GB RAM), confirm that Koopman is fast to simulate and train.

The three datasets, the models, the training and the comparison scripts (including RK4) have all been open-sourced¹.

V. MULTI-DOMAIN MARITIME ROBOTICS

To showcase the usability of the Marinarium facility as a multi-domain maritime robotics research arena, we design and execute a rendezvous mission with a heterogeneous fleet of three robots across three environments. The three platforms, an AUV, an USV, and an UAV, are depicted in Figure 7, together with the ground station used for remote communication with an off-site operator. The setup is very similar to that in [10], with the difference that untethered communication with the AUV can be achieved due to the stones on the tank floor.

A. THE HETEROGENOUS MULTI-ROBOT FLEET

The three vehicles and the ground station are introduced below.

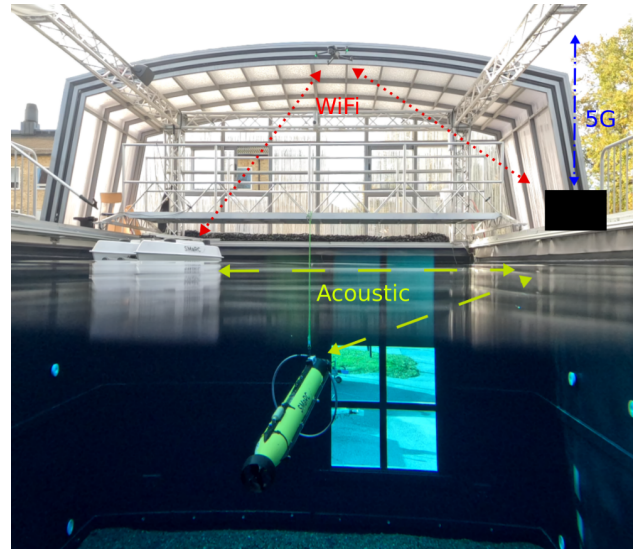


FIGURE 7. Example of a multidomain experimental setup with an AUV, a USV and a UAV linked through three communications channels across the aerial, surface and underwater environments. The black box represents a ground station.

The SAM AUV

SAM is a small, non-holonomic, slender-type AUV developed by the Swedish Maritime Robotics Center (SMaRC) [74]. It is equipped with two counter-rotating propellers within a thrust-vectoring system for steering, and two internal actuators: i) a Variable Buoyancy System (VBS) and ii) a Longitudinal Center of Gravity (LCG) system (by a moving battery pack). Its sensor suite consists of a Waterlinked A50 Doppler Velocity Log (DVL), a pressure sensor, a GPS module, a STIM300 IMU and SBG Attitude and Heading Reference System (AHRS), a Deep Vision side-scan sonar, and three forward-facing cameras. In the communications bay, it carries a 5G and WiFi modem as well as a Suckerfish Delphis underwater acoustic modem. SAM’s navigation architecture consists of an MPC controller based on its dynamics model, which follows Equation (1), equivalent to that in [75], together with a factor graph-based state estimator as in [76] to achieve autonomous waypoint navigation.

The FloatSAM USV

FloatSAM is a small, catamaran-shaped USV of approximately 0.6×0.4 m surface developed by SMaRC. It is equipped with differential thrusters and a PixHawk 6X-Mini controller running PX4 [69] for low-level actuation control. Its sensor suite encompasses a Nortek DVL, a STIM IMU, and a RTK GPS. Regarding communications, FloatSAM carries a 5G modem, a Suckerfish Delphis underwater acoustic modem and a WiFi antenna.

The Crazyflie UAV

The Crazyflie 2.1+ is a lightweight, low-cost UAV by Bitcraze. Its native software stack implements waypoint

¹Code available at: https://github.com/ViktorNfa/bluerov2_dynamics.

(WP) navigation through a combination of PID-controllers and an Extended Kalman Filter (EKF) for localization used to fuse the detections from the surface MoCap.

The Ground Station

The ground station is a portable, waterproof communication module developed to provide a link between a remote operator and vehicles in the field. It is equipped with a Raspberry Pi 4 connected to 5G and Succorfish modems and omnidirectional WiFi.

B. ACROSS-DOMAIN COMMUNICATION LINKS

Every platform in our setup implements ROS 2 as middleware. However, for inter-platform communication, three different links have been established consisting of a physical channel and messaging protocol, depending on the domain. These are depicted in Figure 7 for visualization:

- WiFi/Bluetooth-ROS2 (red): all platforms within WiFi reach (or Bluetooth in the case of the Crazyradio) can communicate with each other directly through ROS 2. This includes SAM while on the surface.
- 5G-MQTT (blue): a NodeRED-based GUI hosted on a cloud server allows off-site users to interact with the vehicles through an MQTT link between the users and the ground station. An MQTT-ROS2 bridge in the ground station allows the user commands to be parsed into ROS 2 messages.
- Acoustic-NM (yellow): the Network Manager (NM) in [77] has been implemented and instantiated per vehicle to parse ROS 2 messages into low-level data frames. These are then scheduled and transferred through the acoustic link provided by the Succorfish modems between underwater platforms.

C. RESULTS AND DISCUSSION

When commanded by an off-site operator, the AUV and the UAV receive the position of the loitering USV tracked by the surface and underwater MoCaps, respectively. They both then proceed to approach the USV and the mission finishes when the UAV has landed on the USV and SAM has maneuvered underneath it.

A timelapse of the RViz visualization of the mission is shown in Figure 8. This visualization was produced by merging and replaying the rosbags collected by the vehicles and the MoCaps. Upon reception of the start command, the UAV takes off vertically from the launch pad (red), travels at a constant altitude over the water to the coordinates of the USV, and lands vertically on the 0.5×0.4m pad (blue) mounted on it. In parallel, when the AUV receives the command over the acoustic link, it navigates towards the USV and dives beneath it until a predefined distance threshold is reached. It then empties its VBS and surfaces, ending the mission.

The scenario presented illustrates how a full inter-domain mission with a heterogeneous fleet of vehicles can be tested

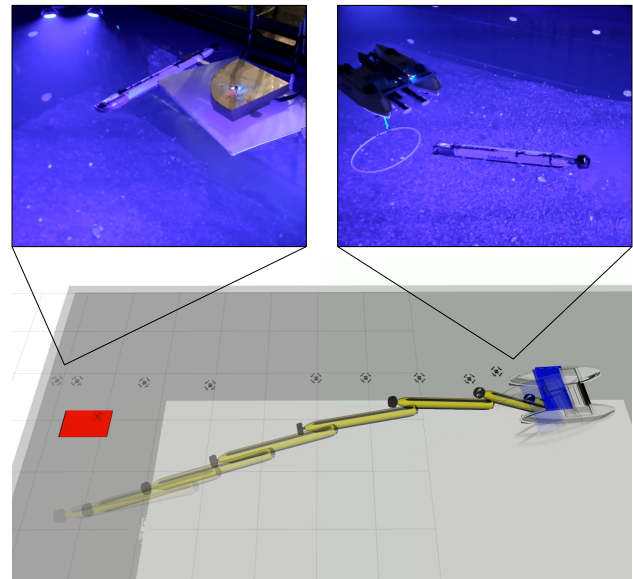


FIGURE 8. Time-lapse RViz visualization of the multi-domain experiment. The Crazyflie UAV takes off from the launchpad (red) and lands on the FloatSAM USV pad (blue). In parallel, the SAM AUV dives towards FloatSAM and soft-docks underneath. On top, two real snapshots of the experiment.

in a controlled facility before field deployment, reducing operational costs, development time, and helping bridge the gap between development in simulation and field testing.

VI. UNDERWATER SIM-TO-REAL GAP BRIDGING

Improving a robot simulator by injecting a learned residual physics model of the real robot, as in [64, 65], requires a system capable of comparing synchronized state information of the real platform with that of its simulation. For this purpose, we utilize the Marinarium digital twin in the SMaRCSim simulator [5], in Figure 1, with a ROS 2-Unity bridge.

A. RESIDUAL DYNAMICS PROBLEM DEFINITION

To demonstrate the applicability of the Marinarium to realizing this sim2real technique underwater, we aim to model the discrepancy between the observed 3D motion of the AUV SAM navigating in the Marinarium and the motion predicted by its simulation model directly from experimental data. The regressed model is then injected into the original simulation to align its behavior more closely with that of the real platform, thereby reducing the sim2real gap. More formally, if we represent the dynamics of the SAM AUV in the SMaRCSim as $\dot{\nu}_k^{sim} = f_s^{sim}(\eta_k, \nu_k, \mathbf{u}_k)$ and equivalently the true dynamics of SAM in the tank via f_s^{real} , the goal is to match the dynamics of f_s^{real} by adding a residual velocity correction to f_s^{sim} , named δ_k .

We express the discrete-time dynamics of SAM by applying a one-step Euler discretization to f_s^{sim} , which serves as the nominal physics model, i.e.

$$\nu_{k+1}^{sim} = \nu_k^{sim} + \Delta_t f_s^{sim}(\eta_k, \nu_k, \mathbf{u}_k) \quad (14)$$

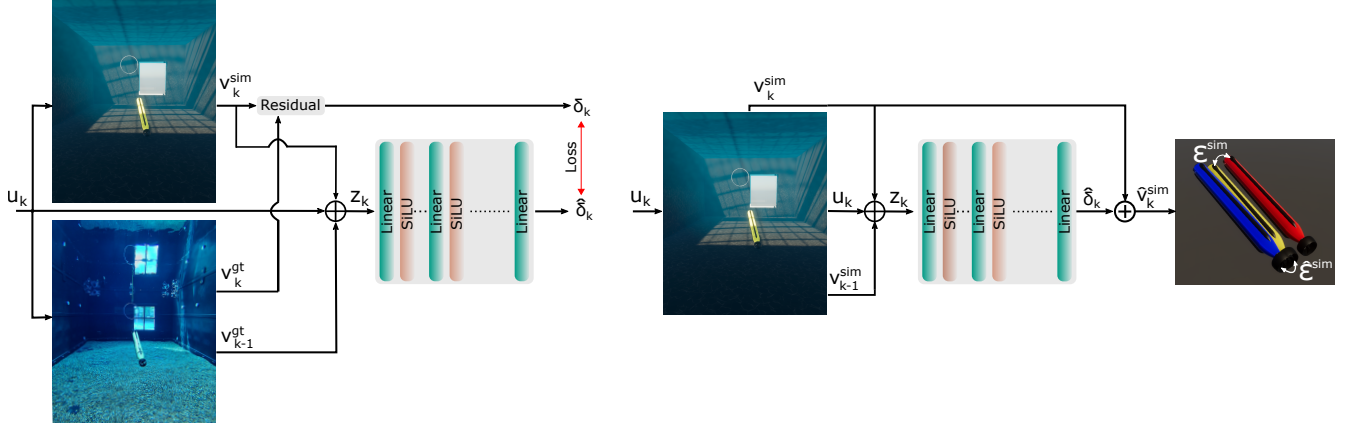


FIGURE 9. Left: the proposed dynamics residual learning pipeline during training with the AUV SAM. The GT and sim velocities from the MoCap and the simulator are used to compute the original residual δ_k over a set of AUV trajectories. A neural network is used to predict the residual $\hat{\delta}_k$ given the state and control input, concatenated in z_k , of the real AUV, and the difference is used to train the NN. Right: during inference, the NN is fed z_k from the original simulated vehicle (yellow), with a motion error ϵ^{sim} when compared to the real vehicle motion (red). The predicted residual is then injected, resulting in a residual-corrected model (blue) with a smaller motion error $\hat{\epsilon}^{sim}$.

The MoCap system provides high-quality measurements of the vehicle's velocity twist, which we use as ground truth and denote by ν_k^{gt} . We also denote by ν_k^{sim} the twist predicted by the simulation model in Equation (14) in the absence of residuals. This allows us to compute the residual directly from data as $\delta_k = \nu_k^{gt} - \nu_k^{sim}$.

B. DATASET CURATION

To learn the residual δ_k , we require a dataset of the form $\mathcal{D}_K = \{\nu_k^{gt}, \nu_k^{sim}, \phi_k, \theta_k, \mathbf{u}_{0:K-1}\}$ for $k = [0 \dots K]$. The predicted velocities ν^{sim} are obtained directly from the simulator by single-step rollouts using the known pose, velocities and control inputs at step k , while the ground-truth velocities ν^{gt} are computed by numerically differentiating the MoCap pose measurements η^{gt} . The MoCap data was first manually cleaned, to remove any tracking errors. To preserve the generality of the representation, we use body-frame ν_k for learning.

Given that the elements of ν_k corresponding to the actuated DoF of SAM will generally be of larger magnitude than the rest, we first normalize (z-score) the velocities per feature. We similarly normalize \mathbf{u}_k per-feature over \mathcal{D}_K . All velocities, both in sim and real, are normalized jointly so all velocities share the same distribution.

We further compute the element-wise mean and standard deviation of δ across \mathcal{D}_K : $\mu_\delta = \mathbb{E}[\delta]$, $\sigma_\delta = \sqrt{\mathbb{V}[\delta]}$, to create the supervised, z-scored residual target:

$$\tilde{\delta}_k = \frac{\delta - \mu_\delta}{\sigma_\delta}$$

C. RESIDUAL DYNAMICS REGRESSION

We apply a Multilayer Perceptron (MLP) architecture to learn the single-step target δ . Our Neural Network (NN) π_θ , depicted in Figure 9, consists of 4 blocks, each containing a linear layer with 256 neurons and SiLU activation functions, applied to all the layers except the last one. At

every timestep, the input layer in π_θ takes in the vector $z_k = [\nu_{k-1}^{gt}, \nu_k^{sim}, \mathbf{u}_k]$ and outputs the inferred residual $\hat{\delta}_k$ such as

$$\hat{\delta}_k = \pi_\theta(z_k)$$

D. TRAINING

To minimize the effect of any remaining undetected outliers in the data, during training the target function is a Huber loss [78] with $\beta = 0.9$:

$$\mathbf{r}_k = \pi_\theta(z_k) - \tilde{\delta}_k \quad (15)$$

$$\mathcal{L}_\beta(r_k) = \begin{cases} \|r_k\|_2^2, & \text{if } \|r\| \leq \beta, \\ \beta * (\|r_k\| - \frac{\beta}{2}), & \text{if } \|r\| > \beta \end{cases} \quad (16)$$

We minimize Equation (16) with AdamW [79] and mini-batches $\mathcal{B} = \{r_n\}_{n=0}^N$ of size $N = 768$, applying a weight decay of 10^{-5} , a learning rate of $3e^{-3}$, and an exponential scheduler with $\gamma = 0.997$ and epochs = 2000, as follows:

$$\hat{\theta} = \arg \min_{\theta} \frac{1}{N} \sum_n \mathcal{L}_\beta(r_n) \quad (17)$$

The training pipeline is depicted in Figure 9, on the left side.

E. INFERENCE

The inference pipeline is depicted in Figure 9, on the right side. At inference time, the NN employs the simulated velocity ν_k^{sim} instead of ν_k^{gt} . ν_{k+1}^{sim} is computed by adding $\hat{\delta}_k$ to the physics in the simulator (PhysX). The NN output is then mapped back to the un-normalized velocity residual (physical units). After computing ν_k^{sim} as described in Equation (14), the corrected simulated velocity during inference is computed as follows:

$$\hat{\nu}_k^{sim} = \nu_k^{sim} + \hat{\delta}_k \quad (18)$$

F. RESULTS AND DISCUSSION

The dataset used for initial experiments consists of 8 different recordings of SAM moving through the tank, separated into 24 different segments, based on cuts required for removing MoCap errors. We used the simulator to resample the data at a constant timestep of 0.02 (50hz), producing a total of 73294 ground truth timesteps equivalent to approximately 24 minutes of real-time operation. To build the \mathcal{D}_K we picked the latest value from each corresponding datastream. Note that the MoCap data rate² exceeds that of the simulator's, so we did not produce repeated datapoints between successive timesteps. Out of the 73294 steps, $K = 65096$ were used for training, while two segments totaling 8198 timesteps were used for evaluation.

The evaluation of the resulting corrected velocities follows the methodology outlined in Section D, with $H \in \{1, 10, 100, 500\}$ and $N = 7998$ trajectories from the dataset.

TABLE 4. Evaluation of the residual (res) vs the original (sim) models over 7998 trajectories. RMS of rollout trajectory endpoint errors over time horizon H. Note that a lower number of 7198 trajectories was used for H = 500.

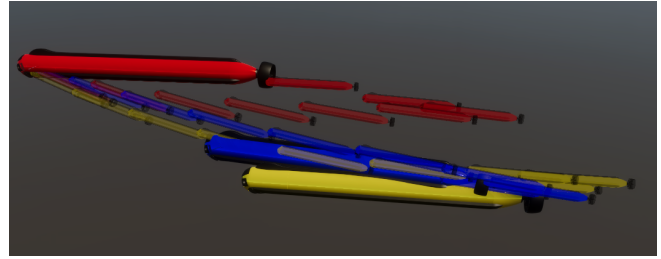
H	\hat{p}^{sim}	p^{sim}	$\hat{\mu}^{sim}$	μ^{sim}	\hat{v}^{sim}	v^{sim}	$\hat{\omega}^{sim}$	ω^{sim}
1	0.00	0.05	0.00	0.14	0.02	0.06	0.08	0.09
10	0.02	0.05	0.38	0.42	0.07	0.12	0.19	0.20
100	0.20	0.30	0.85	1.20	0.20	0.27	0.23	0.25
500	0.32	0.72	0.87	1.20	0.17	0.32	0.25	0.27

Table 4 shows the RMSE of the endpoint pose and velocity components of the overall state error at time horizon $k + H$, for both the normal simulation model $\epsilon_{k+H}^{sim} = \mathbf{x}_{k+H}^{gt} - \mathbf{x}_{k+H}^{sim}$ and residual corrected physics model $\hat{\epsilon}_{k+H}^{sim} = \mathbf{x}_{k+H}^{gt} - \hat{\mathbf{x}}_{k+H}^{sim}$. The endpoint is determined by initiating from MoCap ground-truth \mathbf{x}_k^{gt} and rolling out up to the residual-corrected $\hat{\mathbf{x}}_{k+H}^{sim}$ and un-corrected \mathbf{x}_{k+H}^{sim} vehicles states, which are computed integrating Equation (18).

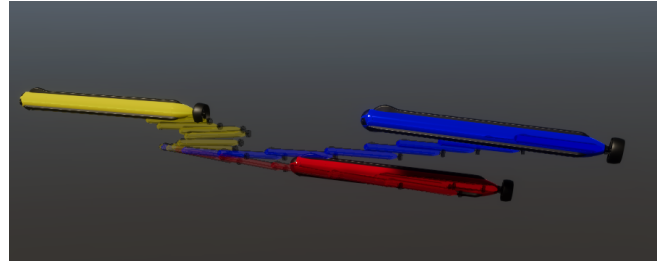
From the quantitative results above it can be seen that the poses and linear velocity errors show overall improvements for longer time horizons. However, we note that there is no significant reduction in angular velocity error. Furthermore, qualitative observations show that when the motion includes significant turns with high angular velocity and sharp changes in forward momentum, the model can become unstable and accelerate in an uncontrollable manner. To illustrate this, we provide two trajectories in Figure 10 - one good and one with a relatively poor performance.

Overall, our results highlight the feasibility and potential of applying real-to-sim techniques through the combination of the Marinarium and the SMarCSim to produce more realistic underwater simulators. The simple methodology presented to exemplify this already offers considerable improvements to the raw simulation model. However, for real-world deployment, robustness would need to be improved

²The MoCap Data rate is approximately 100 Hz in most rosbags. In practice it varies around 90-110Hz, depending on error rate.



(a) Example evaluation trajectory with an effective residual correction. Reversing with a slow forward acceleration at the end.



(b) Example evaluation trajectory with unstable residual correction. Buoyancy change accompanied by fast forward acceleration.

FIGURE 10. Two extreme examples of residual model evaluation trajectories in the simulator. The ground truth (yellow), original simulation (red) and corrected simulation (blue) trajectories start on the same pose and receive the same control inputs sequence. Intermediate trajectory models scaled down for clarity.

and model instabilities addressed. One idea to achieve a more robust model could be to separate the linear and angular components and model their residuals separately. Alternatives also include recursive neural network architectures to improve the handling of rapid velocity and actuation changes, improving data coverage of possible state-action pairs or different principles for the training process, such as those inspired by reinforcement learning [80] or DAgger (Dataset Aggregation) [81].

VII. UNDERWATER VALIDATION OF SPACECRAFT AUTONOMY

Building on the parallels between neutrally buoyant vehicles and free-flying spacecraft, we harness the connection between the Marinarium and the KTH space robotics laboratory [22] to investigate how underwater platforms can be used to validate spacecraft guidance and control algorithms. Neutral buoyancy enables full 6-DoF actuation and weightless behavior, similar in spirit to the neutral-buoyancy environments used for astronaut training, while hydrodynamic effects introduce the main deviations from true microgravity. To give an initial assessment of how well a space control architecture transfers across domains, we conduct paired experiments in which an underwater ROV and a planar space-robot emulator execute the same autonomous inspection task under an identical software and control stack as shown in Figure 4.

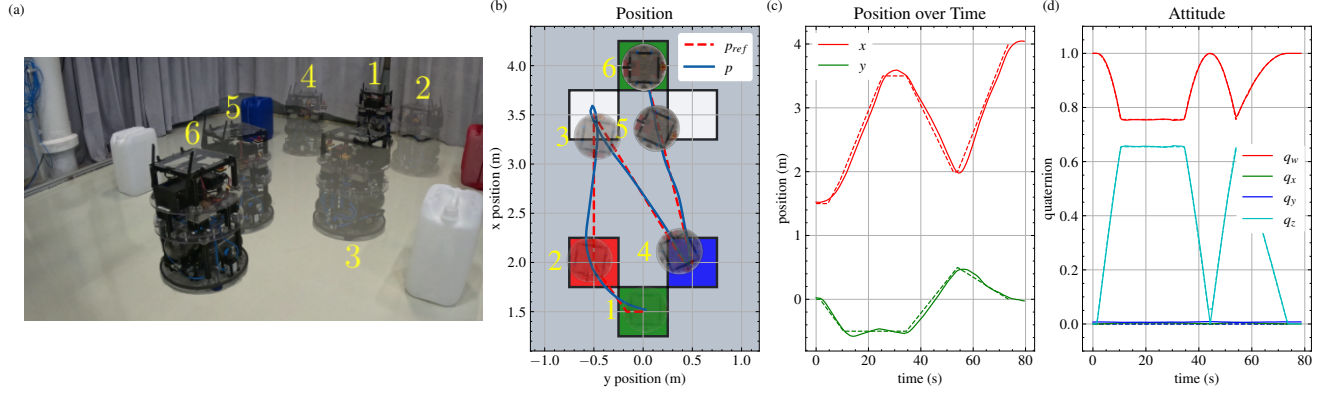


FIGURE 11. Result from the spacecraft-autonomy experiment using the ATMOS free-flyer. The robot is tasked with inspecting a blue object, a red object, and one of two white objects, followed by moving to a final pose, captured in an STL specification. The motion plan is restricted to a 2D plane. a) Time-lapse from the experiment. b) Top-view trajectory of the executed path. c) Position over time. d) Orientation over time.

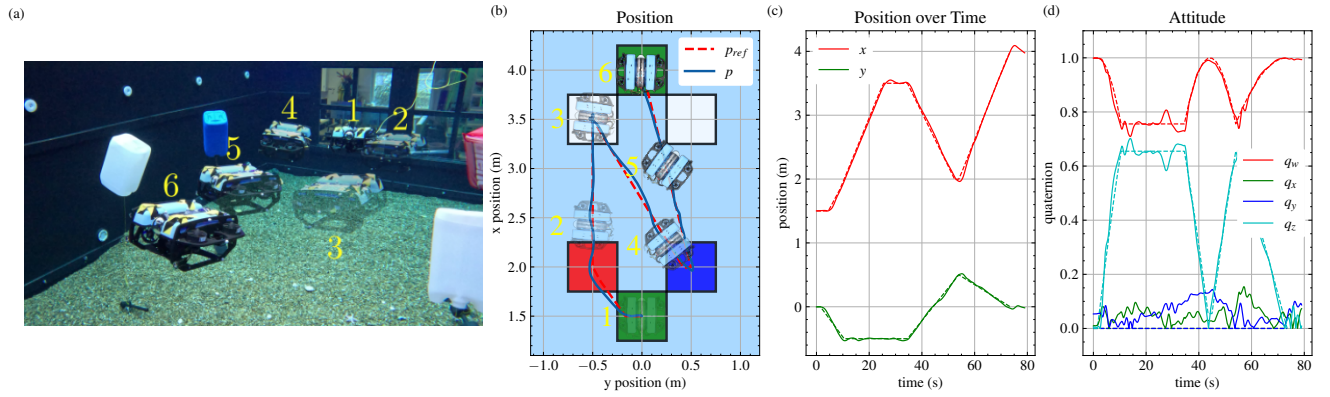


FIGURE 12. Results from the same spacecraft-autonomy task shown in Figure 11, but executed with a BlueROV underwater robot using the same controller and STL-based plan. Although the plan is two-dimensional, the experimental data reveal some motion in all six dimensions.

A. EXPERIMENTAL PLATFORMS AND CONTROL ARCHITECTURE

As introduced in Section III, a set of BlueROV2 Heavy configuration underwater vehicles have been modified to act as underwater surrogates of ATMOS platforms. The ATMOS vehicle floats on air bearings over an epoxy-coated floor, providing nearly frictionless planar 3-DoF motion control through eight compressed-air thrusters. The BlueROV2 Heavy is equipped with eight bidirectional propellers that enable full 6-DoF motion underwater. For comparability, only planar trajectories are commanded during this experiment to match the ATMOS configuration.

B. CONTROLLER FORMULATION

Both systems are controlled using the same 6-DoF free-flyer dynamics model. Translational motion is expressed in the inertial frame through the position \mathbf{p} , while the linear velocity \mathbf{v} is expressed in the body frame. Attitude is parameterized by a unit quaternion \mathbf{q} describing the rotation from the body frame to the inertial frame, with the corresponding rotation matrix denoted $R(\mathbf{q})$. The state is then defined as

$$\mathbf{x} \doteq [\boldsymbol{\eta}^\top, \boldsymbol{\nu}^\top]^\top \doteq [\mathbf{p}^\top, \mathbf{q}^\top, \mathbf{v}^\top, \boldsymbol{\omega}^\top]^\top \in \mathbb{R}^{13},$$

and the control input is defined as $\mathbf{w} = [\mathbf{f}^\top, \boldsymbol{\tau}^\top]^\top$ with \mathbf{f} and $\boldsymbol{\tau}$ the commanded body frame force and torque. The Newton-Euler equations of motion are

$$\dot{\mathbf{p}} = R(\mathbf{q})\mathbf{v} \quad (19a)$$

$$\dot{\mathbf{q}} = \frac{1}{2}\Omega(\boldsymbol{\omega})\mathbf{q} \quad (19b)$$

$$\dot{\mathbf{v}} = \frac{1}{m}(\mathbf{f} + R(\mathbf{q})^\top \mathbf{f}_d) \quad (19c)$$

$$\dot{\boldsymbol{\omega}} = J^{-1}(\boldsymbol{\tau} + \boldsymbol{\tau}_d - \boldsymbol{\omega} \times J\boldsymbol{\omega}) \quad (19d)$$

where m is the vehicle mass, J is the inertia matrix, and $\boldsymbol{\omega}$ is the body-frame angular velocity. External disturbances and model mismatches (including hydrodynamic effects) are represented by the forces \mathbf{f}_d and torques $\boldsymbol{\tau}_d$. The operator $\Omega(\boldsymbol{\omega})$ denotes the quaternion kinematic matrix built from the angular velocity. This model captures the essential inertial, torque-driven motion of a free-flying spacecraft while allowing both platforms to be controlled using an identical NMPC formulation.

High-level force and torque commands are computed by solving a nonlinear MPC problem formulated as the

following optimal control problem (OCP):

$$J^*(x_k) = \min_{\mathbf{w}_k} \sum_{n=0}^{N-1} \ell(\mathbf{x}(n|k), \mathbf{w}(n|k)) + \ell_f(\mathbf{x}(N|k)) \quad (20a)$$

$$\text{s.t. } \mathbf{x}(0|k) = \mathbf{x}_k \quad (20b)$$

$$\mathbf{x}(n+1|k) = f(\mathbf{x}(n|k), \mathbf{w}(n|k)) \quad (20c)$$

$$\mathbf{x}(n|k) \in \mathbb{X}, \quad \mathbf{w}(n|k) \in \mathbb{U}. \quad (20d)$$

The nonlinear dynamics function $f(\cdot)$ is obtained by discretizing the continuous-time model Equation (19) with a sampling time T_s . The sets \mathbb{X} and \mathbb{U} encode state and input constraints such as workspace limits and actuator bounds. The stage and terminal costs $\ell(\cdot)$ and $\ell_f(\cdot)$ penalize deviations from a reference trajectory

$$\ell(\mathbf{x}, \mathbf{w}) = \|\mathbf{x} - \mathbf{x}_r\|_Q^2 + \|\mathbf{w} - \mathbf{w}_r\|_R^2, \quad (21)$$

$$\ell_f(\mathbf{x}) = \|\mathbf{x} - \mathbf{x}_r\|_P^2, \quad (22)$$

with positive semi-definite weighting matrices Q, R, P .

The OCP is solved in real time using ACADOS [82], and the resulting control inputs are transmitted to the micro-controller which allocates the actuators such that the desired force and torque is achieved on either space- or underwater platform. An EKF estimates external disturbance forces and torques during operation, which primarily affect the ROV due to unmodeled hydrodynamic effects, parameter uncertainties, and tether disturbances. The shared control layout is shown in Figure 4.

Both platforms execute a planned trajectory that satisfies a complex inspection task formulated as a Signal Temporal Logic specification [83]. The specification requires sequential inspection of the blue, the red, and either of the white objects (with some temporal flexibility) in a planar workspace. The plan is defined in two dimensions to allow direct comparison of the systems' behavior.

C. RESULTS AND DISCUSSION

The resulting position and attitude trajectories are shown in Figure 11 and Figure 12. Both platforms successfully track the STL-generated plan and exhibit similar overall motion profiles, demonstrating that the underwater system can reproduce the behavior of a free-flying spacecraft under the same control architecture. The tracking errors w.r.t. the reference trajectory are highlighted in Figure 13. The BlueROV2 displays small oscillations in attitude, which are expected due to unmodeled hydrodynamic forces and residual tether disturbances. Nevertheless, its trajectory remains consistent with the reference, validating the feasibility of underwater testing for spacecraft guidance and control methods.

These results highlight the feasibility of using underwater systems to validate spacecraft guidance and control algorithms under realistic dynamic conditions. Extending this approach to six degrees of freedom, including active compensation of known hydrodynamic effects, and establishing formal guarantees for equivalence between underwater

and space-domain validation, represent important research directions for these facilities.

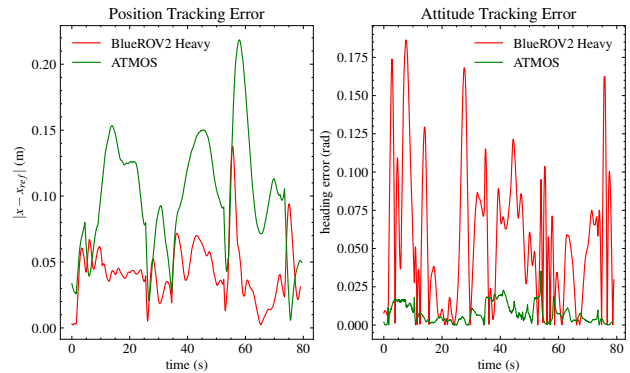


FIGURE 13. Tracking errors of the space validation experiment on the ATMOS free-flyer and the BlueROV.

VIII. CONCLUSION

This work has introduced the Marinarium, a new modular and cost-effective underwater robotics research facility designed to advance the development of marine and space robotics from campus. We argue that the thoughtful and tight design of the facility reduces the traditional economic and logistical barriers that separate laboratory research from field experimentation. By prioritizing minimal construction and operating cost alongside high-fidelity sensing and a flexible setup, the Marinarium demonstrates that realistic field experimentation in these domains need not be prohibitively complex or expensive.

Through four sets of experiments, we have demonstrated how this facility can bring the traditionally hard to access maritime and space domains closer to the field robotics research community by providing: i) the capacity to collect high-quality observations of underwater vehicles behavior, ii) a fully-monitored, multi-domain testing volume with controllable access to real weather conditions, iii) a simulation environment that can be enhanced through real-to-sim techniques, and iv) a validation testbed for space robotics through underwater surrogates.

Furthermore, our experiments have yielded the following contributions:

- A novel application of the Koopman operator for system identification of UW vehicles that significantly enhances the accuracy with which the vehicle state can be predicted for extended time into the future. The comparison to multiple baselines also shows the necessity for further research for UW modeling.
- A demonstration of a multi-domain collaborative task, where the UAV, USV, and AUV are all tracked precisely by the Marinarium's dual UW and AW MoCap for further evaluation. Extension to include additional robots/vehicles as well as divers is supported.

- The first example of improving an UW robot simulator by injecting a learned dynamics residual model, made possible by the accurate tracking in the Marinarium, significantly improves simulation of the AUV, thus considerably reducing the sim2real gap for UW vehicles.
- The uniquely connected UW and space laboratories allowed the STL trajectory tracking performance of a spacecraft emulated by a free-flyer platform to be validated directly on and UW vehicle.

These results highlight how by deliberately coupling precise sensing, cross-domain access, and simulation integration, the Marinarium enables new experimental methodologies that bridge laboratory robotics, offshore operations, and space applications.

REFERENCES

- [1] Enrica Zereik, Marco Bibuli, Nikola Mišković, Pere Ridaó, and António Pascoal. Challenges and future trends in marine robotics. *Annual Reviews in Control*, 46:350–368, 2018.
- [2] Martin Aubard, Ana Madureira, Luís Teixeira, and José Pinto. Sonar-based deep learning in underwater robotics: Overview, robustness, and challenges. *IEEE Journal of Oceanic Engineering*, 2025.
- [3] Patrick W Kenneally, Scott Piggott, and Hanspeter Schaub. Basilisk: A flexible, scalable and modular astrodynamics simulation framework. *Journal of aerospace information systems*, 17(9):496–507, 2020.
- [4] Sara Aldhaferi, Yang Hu, Yongchang Xie, Peng Wu, Dimitrios Kanoulas, and Yuanchang Liu. Underwater robotic simulators review for autonomous system development. *arXiv preprint arXiv:2504.06245*, 2025.
- [5] Mart Kartašev, David Dörner, Özer Özkahraman, Petter Ögren, Ivan Stenius, and John Folkesson. SMaRC-Sim: Maritime Robotics Simulation Modules. In *2025 Symposium on Maritime Informatics and Robotics (MARIS)*, pages 1–4, June 2025.
- [6] Musa Morena Marcusso Manhães, Sebastian A Scherer, Martin Voss, Luiz Ricardo Douat, and Thomas Rauschenbach. Uuv simulator: A gazebo-based package for underwater intervention and multi-robot simulation. In *Oceans 2016 Mts/Ieee Monterey*, pages 1–8. Ieee, 2016.
- [7] Sebastian Höfer, Kostas Bekris, Ankur Handa, Juan Camilo Gamboa, Melissa Mozifian, Florian Golemo, Chris Atkeson, Dieter Fox, Ken Goldberg, John Leonard, et al. Sim2real in robotics and automation: Applications and challenges. *IEEE transactions on automation science and engineering*, 18(2):398–400, 2021.
- [8] Kevin Chang, Rakesh Vivekanandan, Noah Pragin, Sean Bullock, and Geoffrey Hollinger. Learning to dock: A simulation-based study on closing the sim2real gap in autonomous underwater docking. *arXiv preprint arXiv:2506.17823*, 2025.
- [9] Artur K. Lidtke, Douwe Rijkema, and Bülent Düz. General reinforcement learning control for AUV manoeuvring in turbulent flows. *Ocean Engineering*, 309:118538, October 2024.
- [10] Joel Lindsay, Jordan Ross, Mae L Seto, Edward Gregson, Alexander Moore, Jay Patel, and Robert Bauer. Collaboration of heterogeneous marine robots toward multidomain sensing and situational awareness on partially submerged targets. *IEEE Journal of Oceanic Engineering*, 47(4):880–894, 2022.
- [11] Fausto Ferreira, Juraj Obradović, Dula Nad, Ivan Lončar, Luka Mandić, Igor Kvasić, Natko Kraševac, and Nikola Mišković. Remote-access marine robotics infrastructure and experiments at labust. *Journal of marine science and engineering*, 12(2):317, 2024.
- [12] James C Kinsey, David A Smallwood, and Louis L Whitcomb. A new hydrodynamics test facility for uuv dynamics and control research. In *Oceans 2003. Celebrating the Past... Teaming Toward the Future (IEEE Cat. No. 03CH37492)*, volume 1, pages 356–361. IEEE, 2003.
- [13] Marios Xanthidis, Nare Karapetyan, Hunter Damron, Sharmin Rahman, James Johnson, Allison O’Connell, Jason M O’Kane, and Ioannis Rekleitis. Navigation in the presence of obstacles for an agile autonomous underwater vehicle. In *2020 IEEE International Conference on Robotics and Automation (ICRA)*, pages 892–899. IEEE, 2020.
- [14] Zhizun Xu, Maryam Haroutunian, Alan J Murphy, Jeff Neasham, and Rose Norman. An integrated visual odometry system with stereo camera for unmanned underwater vehicles. *IEEE Access*, 10:71329–71343, 2022.
- [15] Levi Cai, Kevin Chang, and Yogesh Girdhar. Learning to swim: Reinforcement learning for 6-dof control of thruster-driven autonomous underwater vehicles. In *2025 IEEE International Conference on Robotics and Automation (ICRA)*, pages 11286–11293. IEEE, 2025.
- [16] Guanda Li, Jun Shintake, and Mitsuhiro Hayashibe. Deep reinforcement learning framework for underwater locomotion of soft robot. In *2021 IEEE international conference on robotics and automation (ICRA)*, pages 12033–12039. IEEE, 2021.
- [17] Yu-Hsien Lin, Chen-Hao Chiang, Chao-Ming Yu, and Joyce Yi-Tzu Huang. Intelligent docking control of autonomous underwater vehicles using deep reinforcement learning and a digital twin system. *Expert Systems with Applications*, 296:129085, 2026.
- [18] C.R. Carignan and D.L. Akin. The reaction stabilization of on-orbit robots. *IEEE Control Systems Magazine*, 20(6):19–33, 2000.
- [19] Christian Ernst Siegfried Koch, Marko Jankovic, Sankaranarayanan Natarajan, Shubham Vyas, Wiebke Brinkmann, Vincent Bissonnette, Thierry Germa, Alessio Turetta, and Frank Kirchner. Underwater

- demonstrator for autonomous in-orbit assembly of large structures. In *15th International Symposium on Artificial Intelligence, Robotics and Automation in Space (i-SAIRAS)*, pages 1–8, 2020.
- [20] Jean-Bruno Marciacq and Loredana Bessone. Crew training safety: An integrated process. In *Safety design for space systems*, pages 745–815. Elsevier, 2009.
- [21] Michael J Neufeld and John B Charles. Practicing for space underwater: inventing neutral buoyancy training, 1963–1968. *Endeavour*, 39(3-4):147–159, 2015.
- [22] Pedro Roque, Sujet Phodapol, Elias Krantz, Jaeyoung Lim, Joris Verhagen, Frank J Jiang, David Dörner, Huina Mao, Gunnar Tibert, Roland Siegwart, et al. Towards open-source and modular space systems with atmos. *arXiv preprint arXiv:2501.16973*, 2025.
- [23] SINTEF Ocean. Ocean Laboratory. <https://www.sintef.no/en/all-laboratories/ocean-laboratory/>, 2025. Accessed: 2025-11-18.
- [24] Technology Centre for Offshore & Marine (TCOMS). Research & development on ocean systems and solutions. <https://tcoms.sg/website/research-development/>, 2025. Accessed: 2025-11-18.
- [25] Ifremer, Recherches et Développements Technologiques. Deep wave basin in brest. <https://rd-technologiques.ifremer.fr/Moyens/Bassins-Canal-d-Essais/Bassin-d-essais-du-centre-de-Bretagne#Domaines>. Accessed: 2025-11-26.
- [26] Dalhousie University. Aquatron laboratory - pool tank. https://www.dal.ca/dept/aquatron/facilities/pool_tank.html. Accessed: 2025-11-25.
- [27] Peter Gunnarson and John O Dabiri. Fish-inspired tracking of underwater turbulent plumes. *Bioinspiration & Biomimetics*, 19(5):056024, 2024.
- [28] University of Michigan. New robotics research water tank to enable advanced marine autonomy. <https://robotics.umich.edu/news/2025/new-robotics-research-water-tank/>.
- [29] BYU, Electrical and Computer Engineering. Auv testing facility and resources. <https://frostlab.byu.edu/tank>. Accessed: 2025-11-26.
- [30] David Akin, Robert Roberts, J. Lane, and Steven Weisman. Robotic capabilities for complex space operations. In *AIAA Space 2001 Conference and Exposition*. American Institute of Aeronautics and Astronautics (AIAA), 2001.
- [31] University of Maryland, Division of Research. Neutral buoyancy research facility (nbrf).
- [32] Juniper C Jairala, Robert Durkin, Ralph J Marak, Stephanie A Sipila, Zane A Ney, Scott E Parazynski, and Arthur H Thomason. Eva development and verification testing at nasa’s neutral buoyancy laboratory. In *42nd International Conference on Environmental Systems (ICES)*, number JSC-CN-26179, 2012.
- [33] DFKI Robotics Innovation Center. Maritime infrastructure, research facilities & labs. <https://robotik.dfki-bremen.de/en/research/research-facilities-labs/maritime-infrastructure>. Accessed: 2025-11-12.
- [34] Fraunhofer IOSB-AST. Research platform for underwater robotics. <https://www.iosb-ast.fraunhofer.de/en/departments/Underwater-Robotics/research-platform-underwater-robotic.html>, 2025. Accessed: 2025-11-18.
- [35] Universitat de Girona. Research center in underwater robotics (cirs). http://eia.udg.es/~pere/Pere_Ridao_Home_Page/CIRS.html. Accessed: 2025-11-25.
- [36] G Monrós-Andreu, S Lopez-Barajas, J Luis-Gómez, R Marín Prades, A González-Barberá, A Macias, A Solis, R Martínez-Cuenca, PJ Sanz, and S Chiva. Surrogate modeling for rov trajectory planning in realistic marine currents: A methodology for data assisted underwater navigation. In *OCEANS 2025 Brest*, pages 1–8. IEEE, 2025.
- [37] INESC TEC. Robotics and autonomous systems laboratory. <https://www.inesctec.pt/en/laboratories/robotics-and-autonomous-systems-laboratory>. Accessed: 2025-11-26.
- [38] AAU Energy Aalborg University. Underwater technology. <https://www.energy.aau.dk/research/research-groups/underwater-technology>. Accessed: 2025-11-26.
- [39] DTU Center for Collaborative Autonomous Systems. DTU ASTA Autonomous Systems Test Arena. <https://asta.dtu.dk/>, 2025. Accessed: 2025-11-20.
- [40] M Mcnutt, G Massion, K Raybould, J Bellingham, and C Paull. Mars: A cabled observatory testbed in monterey bay. In *EGS-AGU-EUG Joint Assembly*, page 11585, 2003.
- [41] Alexandru Umlauf, Felix Schmidt, Gerrit Lünsdorf, Torben Globisch, Nele Daske, Patrick Suhrbier, Kristine Bauer, Sascha Krohmann, and Uwe Freiherr von Lukas. The digital ocean lab (dol): Centralising ocean research in the baltic sea. In *OCEANS 2024-Halifax*, pages 1–6. IEEE, 2024.
- [42] Martin Ludvigsen, Finn Olav Bjørnson, Ingrid Ellingsen, Kay Fjørtoft, Karl Henning Hasle, Hans Petter Hildre, Beate Kvamstad-Lervold, Andreas Madsen, Kjell Olav Skjølsvik, Asgeir J Sørensen, et al. Fjordlab: A full-scale marine field laboratory for innovation, research, and education in ocean science and technology. In *OCEANS 2025 Brest*, pages 1–9. IEEE, 2025.
- [43] Salvador López-Barajas, Sebastian Realpe, Josep Marín, Alejandro Solis, Andrea Pino, Raúl Marín, and Pedro Sanz. Unity-based mixed reality hri for underwater exploration and object recovery using a i-av and hololens. In *OCEANS 2025 Brest*, pages 1–4. IEEE, 2025.

- [44] Jingyu Song, Onur Bagoren, Razan Andigani, Advait Sethuraman, and Katherine A Skinner. Turtlmap: Real-time localization and dense mapping of low-texture underwater environments with a low-cost unmanned underwater vehicle. In *2024 IEEE/RSJ International Conference on Intelligent Robots and Systems (IROS)*, pages 1191–1198. IEEE, 2024.
- [45] Gerald Brantner and Oussama Khatib. Controlling ocean one: Human–robot collaboration for deep-sea manipulation. *Journal of Field Robotics*, 38(1):28–51, 2021.
- [46] Hanzhi Yang and Nina Mahmoudian. Gliding in extreme waters: Dynamic modeling and nonlinear control of an agile underwater glider. *IFAC-PapersOnLine*, 58(20):121–126, 2024.
- [47] Rui Lopes, Arash Eslamdoost, Rikard Johansson, Seemontini RoyChoudhury, Rickard E Bensow, Per Hogström, and Dmitriy Ponkratov. Resistance prediction using cfd at model-and full-scale and comparison with measurements. *Ocean Engineering*, 321:120367, 2025.
- [48] Abdelhakim Amer, David Felsager, Yury Brodskiy, and Andriy Sarabakha. Modelling of underwater vehicles using physics-informed neural networks with control, 2025.
- [49] Chu-Jou Wu. 6-DoF Modelling and Control of a Remotely Operated Vehicle. Master’s thesis, Flinders University, College of Science and Engineering, 2018. Electronic thesis, Flinders University Theses Collection.
- [50] Malte von Benzon, Fredrik Fogh Sørensen, Esben Uth, Jerome Jouffroy, Jesper Liniger, and Simon Pedersen. An open-source benchmark simulator: Control of a bluerov2 underwater robot. *Journal of Marine Science and Engineering*, 10(12), 2022.
- [51] Leif Christensen, José de Gea Fernández, Marc Hildebrandt, Christian Ernst Siegfried Koch, and Bilal Wehbe. Recent advances in ai for navigation and control of underwater robots. *Current Robotics Reports*, 3(4):165–175, 2022.
- [52] Bilal Wehbe and Mario Michael Krell. Learning coupled dynamic models of underwater vehicles using support vector regression. In *OCEANS 2017-Aberdeen*, pages 1–7. IEEE, 2017.
- [53] Abdelhakim Amer, Mohit Mehndiratta, Yury Brodskiy, and Erdal Kayacan. Empowering autonomous underwater vehicles using learning-based model predictive control with dynamic forgetting gaussian processes. *IEEE Transactions on Control Systems Technology*, 33(5):1913–1920, 2025.
- [54] H. Harry Asada and Jose A. Solano-Castellanos. Control-coherent koopman modeling: A physical modeling approach. In *2024 IEEE 63rd Conference on Decision and Control (CDC)*, pages 7314–7319, 2024.
- [55] John McConnell, Armon Shariati, Paul Szenher, and Yaxuan Li. Above and below: Heterogeneous multi-robot slam across surface and underwater domains. *IEEE Robotics and Automation Letters*, 11(1):129–136, 2025.
- [56] Matheus M Dos Santos, Giovanni G De Giacomo, Paulo LJ Drews-Jr, and Silvia SC Botelho. Cross-view and cross-domain underwater localization based on optical aerial and acoustic underwater images. *IEEE Robotics and Automation Letters*, 7(2):4969–4974, 2022.
- [57] UN Trade & Development. Shipping data: Unctad releases new seaborne trade statistics.
- [58] Florian Shkurti, Anqi Xu, Malika Meghjani, Juan Camilo Gamboa Higuera, Yogesh Girdhar, Philippe Giguere, Bir Bikram Dey, Jimmy Li, Arnold Kalmbach, Chris Prahacs, et al. Multi-domain monitoring of marine environments using a heterogeneous robot team. In *2012 IEEE/RSJ International Conference on Intelligent Robots and Systems*, pages 1747–1753. IEEE, 2012.
- [59] Nikolaos Nomikos, Panagiotis K Gkonis, Petros S Bithas, and Panagiotis Trakadas. A survey on uav-aided maritime communications: Deployment considerations, applications, and future challenges. *IEEE Open Journal of the Communications Society*, 4:56–78, 2022.
- [60] Jiqiang Li, Guoqing Zhang, Changyan Jiang, and Weidong Zhang. A survey of maritime unmanned search system: Theory, applications and future directions. *Ocean Engineering*, 285:115359, 2023.
- [61] Harish Anand, Stephen A Rees, Zhiang Chen, Ashwin Jose Poruthukaran, Sarah Bearman, Lakshmi Gana Prasad Antervedi, and Jnaneshwar Das. Open-uav cloud testbed: A collaborative design studio for field robotics. In *2021 IEEE 17th International Conference on Automation Science and Engineering (CASE)*, pages 724–731. IEEE, 2021.
- [62] Elie Aljalbout, Jiaxu Xing, Angel Romero, Iretyayo Akinola, Caelan Reed Garrett, Eric Heiden, Abhishek Gupta, Tucker Hermans, Yashraj Narang, Dieter Fox, et al. The reality gap in robotics: Challenges, solutions, and best practices. *Annual Review of Control, Robotics, and Autonomous Systems*, 9, 2025.
- [63] Vicente Sufán and Giancarlo Troni. Swim4Real: Deep Reinforcement Learning-Based Energy-Efficient and Agile 6-DOF Control for Underwater Vehicles. *IEEE Robotics and Automation Letters*, 10(7):7326–7333, July 2025.
- [64] Elia Kaufmann, Leonard Bauersfeld, Antonio Loquercio, Matthias Müller, Vladlen Koltun, and Davide Scaramuzza. Champion-level drone racing using deep reinforcement learning. *Nature*, 620(7976):982–987, 2023.
- [65] Junpeng Gao, Mike Y Michelis, Andrew Spielberg, and Robert K Katzschmann. Sim-to-real of soft robots with learned residual physics. *IEEE Robotics and*

- Automation Letters*, 2024.
- [66] David P. Miller, Anne Wright, Y Sargent, Rob Cohen, and Teresa Hunt. Attitude and Position Control Using Real-Time Color Tracking. *ResearchGate*, March 2000.
- [67] NASA. Vertical Habitability Layout Studies and Neutral Buoyancy/Parabolic Flight Habitat Studies. Technical Report Document ID: 20230008022, NASA Technical Reports Server., 2014.
- [68] NASA. Nasa analogs and mockups.
- [69] Lorenz Meier, Dominik Honegger, and Marc Pollefeys. PX4: A node-based multithreaded open source robotics framework for deeply embedded platforms. In *2015 IEEE International Conference on Robotics and Automation (ICRA)*, pages 6235–6240, May 2015.
- [70] Thor I. Fossen. *Handbook of Marine Craft Hydrodynamics and Motion Control*. John Wiley & Sons, Ltd., Chichester, UK, 2nd edition, 2021.
- [71] Arthur E. Hoerl and Robert W. Kennard. Ridge regression: Biased estimation for nonorthogonal problems. *Technometrics*, 12(1):55–67, 1970.
- [72] Steven L. Brunton, Marko Budišić, Eurika Kaiser, and J. Nathan Kutz. Modern koopman theory for dynamical systems. *SIAM Review*, 64(2):229–340, 2022.
- [73] Holger Wendland. Computational aspects of radial basis function approximation. In Kurt Jetter, Martin D. Buhmann, Werner Haussmann, Robert Schaback, and Joachim Stöckler, editors, *Topics in Multivariate Approximation and Interpolation*, volume 12 of *Studies in Computational Mathematics*, pages 231–256. Elsevier, 2006.
- [74] Sriharsha Bhat, Ignacio Torroba, Özer Özkahraman, Nils Bore, Christopher Illiffe Sprague, Yiping Xie, Ivan Stenius, Josefine Severholt, Carl Ljung, John Folkesson, et al. A cyber-physical system for hydro-batic auvs: System integration and field demonstration. In *2020 IEEE/OES Autonomous Underwater Vehicles Symposium (AUV)*, pages 1–8. IEEE, 2020.
- [75] Sriharsha Bhat, Chariklia Panteli, Ivan Stenius, and Dimos V Dimarogonas. Nonlinear model predictive control for hydrobatics: Experiments with an under-actuated auv. *Journal of Field Robotics*, 40(7):1840–1859, 2023.
- [76] David Dörner, Aldo Terán Espinoza, Ignacio Torroba, Jakob Kутtenkeuler, and Ivan Stenius. To smooth or to filter: a comparative study of state estimation approaches for vision-based autonomous underwater docking. In *OCEANS 2024-Singapore*, pages 1–9. IEEE, 2024.
- [77] Davide Fenucci, Jeremy Sitbon, Jeffrey Neasham, Alexander B Phillips, and Andrea Munafò. Ad hoc acoustic network aided localization for micro-auvs. *Field Robotics*, 2:1888–1919, 2022.
- [78] Peter J Huber. Robust estimation of a location parameter. In *Breakthroughs in statistics: Methodology and distribution*, pages 492–518. Springer, 1992.
- [79] Ilya Loshchilov and Frank Hutter. Decoupled weight decay regularization. *arXiv preprint arXiv:1711.05101*, 2017.
- [80] Tobias Johannink, Shikhar Bahl, Ashvin Nair, Jianlan Luo, Avinash Kumar, Matthias Loskyll, Juan Aparicio Ojea, Eugen Solowjow, and Sergey Levine. Residual reinforcement learning for robot control. In *2019 International Conference on Robotics and Automation (ICRA)*, pages 6023–6029, 2019.
- [81] Stéphane Ross, Geoffrey J. Gordon, and J. Andrew Bagnell. A reduction of imitation learning and structured prediction to no-regret online learning. In *International Conference on Artificial Intelligence and Statistics*, 2010.
- [82] Robin Verschueren, Gianluca Frison, Dimitris Kouzoupis, Jonathan Frey, Niels van Duijkeren, Andrea Zanelli, Branimir Novoselnik, Thivaharan Albin, Rien Quirynen, and Moritz Diehl. acados – a modular open-source framework for fast embedded optimal control. *Mathematical Programming Computation*, 2021.
- [83] Alexandre Donzé and Oded Maler. Robust satisfaction of temporal logic over real-valued signals. In *International conference on formal modeling and analysis of timed systems*, pages 92–106. Springer, 2010.